CIVIL ENGINEERING JOURNAL

Article no. 20

THE CIVIL ENGINEERING JOURNAL 2-2025

IMPACT OF TERRAIN AND ENVIRONMENT ON THE ACCURACY OF VEHICLE-BASED MOBILE MAPPING SYSTEMS

Lukáš Běloch

Czech Technical University in Prague, Faculty of Civil Engineering, Department of Geomatics, Thákurova 7, Praha 6, Czech Republic; lukas.beloch@fsv.cvut.cz

Received: *14.04.2025*
Received in revised form: *20.06.2025*
Accepted: *24.07.2025*

ABSTRACT

The rapid collection of accurate spatial data and its use in various domains is driving the evolution of Mobile Mapping Systems (MMS). This study evaluates the accuracy of the Riegl VMX-2HA system in three different environments: an urban residential area, an open road section with an unobstructed view of the sky, and a forested roadway where GNSS signals are significantly affected. This research investigates the effect of these environments and different alignment methods on point cloud accuracy. A combination of GNSS, IMU and DMI was used to determine the trajectory, with measurements tied to GCPs. The study compares the results of the processing of the separate sections with the calculation of the entire section and evaluates the differences of the repeated measurements. The results show that aligning measurements without separating sections by environment improves accuracy. The results contribute to the optimisation of MMS-based data collection strategies and provide insight to improve the reliability of spatial data collection.

KEYWORDS

Mobile laser scanning, Mobile mapping system, Point cloud accuracy, Riegl VMX-2HA

INTRODUCTION

The requirement for rapid spatial data collection was behind the creation of the first mobile mapping devices. These devices were initially georeferenced only to ground control points (GCPs); later, additional sensors were integrated for positioning [1; 2; 3]. These methods have a significant impact on overall accuracy. To determine the initial trajectory, a combination of GNSS (Global Navigation Satellite System), IMU (Inertial Measurement Unit), and DMI (Distance Measurement Indicators) are used in vehicle mounted Mobile Mapping Systems (MMS).

Although the GNSS system can achieve absolute centimetre accuracy, the GNSS signal is often degraded by sky obscuration or multipath interference. The IMU is used to obtain accelerations and rotations, and the relative position of the vehicle can be determined from the measurements. However, errors and noise accumulate in these measurements. For optimal computation of the initial trajectory by combining the above methods, it uses the Kalman filter [4; 5; 6]. In addition, the measured trajectory can be transformed into GCPs to ensure accuracy or improve accuracy in sections without a GNSS signal [7; 8]. Another method is to align the point cloud using the Simultaneous Localization and Mapping (SLAM) algorithm [9; 10], but this principle is mostly used for handheld mobile laser scanners, which are mainly used in places without GNSS signals such as buildings [11; 12; 13], forests [14; 15], historical structures [16] or mines [17].

Currently, there are several commercial vehicle-mounted MMS solutions that use panoramic cameras and Light Detection and Ranging (LiDAR) sensors for data acquisition [18]. In testing these devices, the authors of this paper discuss both the accuracy and data quality of the system and its use for specific purposes.

The use of MMS is currently highly relevant. These devices are being developed and improved for several reasons. The first is their use for autonomous vehicle control. This focus involves the relative position of the vehicle (car) in its surroundings, the recognition of traffic signs and the monitoring of traffic [19; 20; 21; 22]. In this context, deep learning tools are widely used for data processing and classification [23; 24; 25; 26; 27; 28].

For surveying purposes, the resulting accuracy of the output is important. In this context, papers deal with the accuracy of the systems [29; 30; 31; 32] especially in terms of the impact of the density of GPSs [33; 34; 35]. These papers imply that the number and quality of GCPs have an important role in the accuracy of the result. However, for effective data collection, it is recommended to use GCPs targeted by the GNSS method with a spacing of 1000 m. This paper focusses on the investigation of the accuracy and behaviour of the MMS device in terrain with different characteristics. [35; 36].

MATERIALS AND METHODS

This chapter describes the characteristics of the test field, the determination of ground point coordinates, and point signalling. Furthermore, it gives a brief description of the work involved in the creation of point clouds, and it concludes with a description of the evaluation of observed values when working with MMS.

Test Field Specification

The test field (Figure 1) dedicated to investigating the properties of the MMS approach using the Riegl VMX-2HA was designed to include various types of area. The test field is in Pilsen, South suburb (Jižní předměstí, 49.7299869N, 13.3574144E). The total length of the test field is 5.5 km with 109 points spaced approximately 50 m apart.

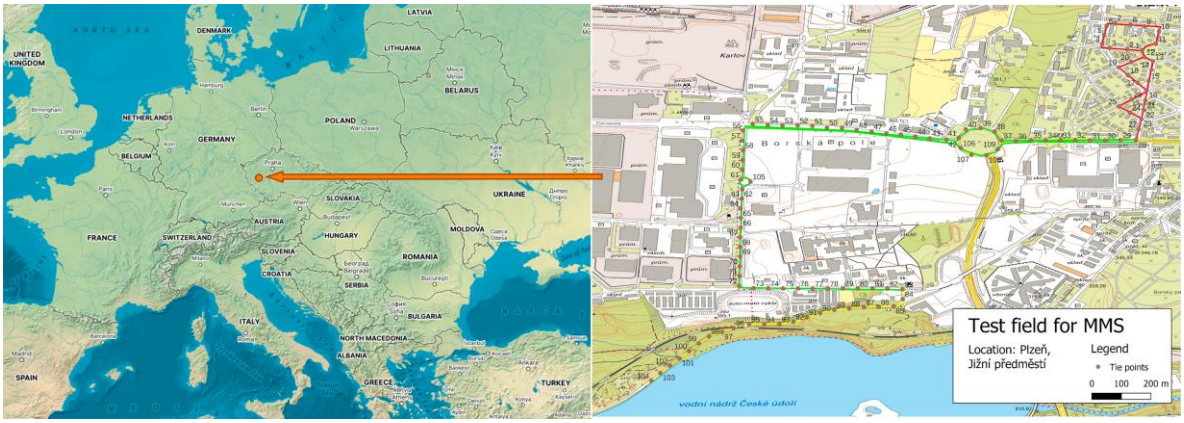

Fig. 1 - Map of the MMS test field

Field Sections

The first section (Figure 2a), 1.5 km long, is in the calm locality of "Na Hvězdě". This area is dominated by residential development and street trees. The second section (Figure 2b) lies along "Sukova", "Folmavská" and "U Letiště" streets and is a multi-lane road with unobstructed views of the sky. The last section of 1 km is then placed in "Dobřanská" Street (Figure 2c). The surrounding area of this street is forested and therefore the GNSS signal is significantly interfered with.

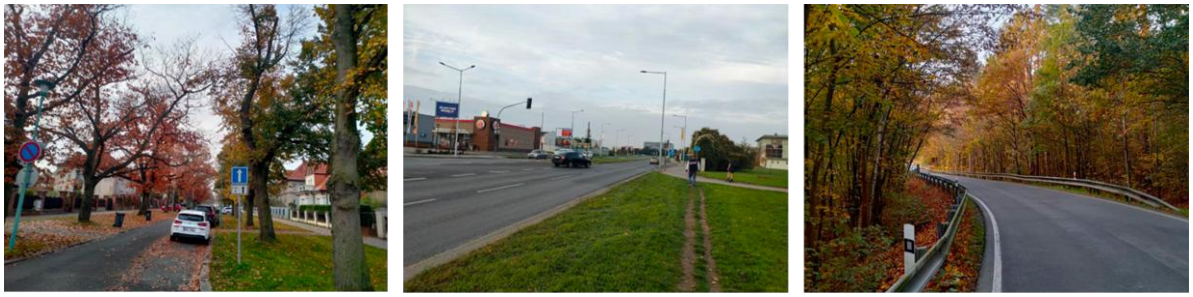

(a) (b) (c)

Fig.2 - Types of area (a – Section 1, b – Section 2, c – Section 3)

Reference and Validation Point Network

Control and check points were stabilised with a measuring steel spike and marked by street lines or a 15x15 cm chequerboard target. The coordinates of the points of all sections were determined by the GNSS RTK method (GNSS points), and the points of the first section were additionally determined by a total station with subsequent alignment (TS points).

Each point was independently measured twice using a Leica GS18. The average standard deviations of the GNSS point determinations were calculated based on these dual measurements. Table 1 presents the standard deviations of the GNSS coordinates derived from the repeated measurements.

Tab.1 - Deviations of GNSS measurement

Field Sections	StDev 2D [mm]	StDev 3D [mm]
Section 1	23	27
Section 2	14	16
Section 3	14	20

Only ground points in Section 1 were measured using the polygon method using a Leica TS1200 total station and then calculated by adjustment in EasyNET software (Version 3.5). Section 1 was assumed to be moderately demanding in terms of GNSS interference. The coordinates determined by this method will be used to calculate the differences between the point-cloud alignment methods. Measuring the entire field using this method would be time consuming, and despite this, it is not expected to be of significant benefit to this work. Table 2 shows the network adjustment parameters in the EasyNet software.

Tab.2 - Adjustment parameters of the tied network

Adjustment method	Tied network
Fixed points	1, 5, 25
Average 2D standard deviation	2.2 mm
Average 3D standard deviation	2.2 mm

Methodology

The data acquisition parameters, the vehicle speed, and the calculation settings affect not only the density of the point cloud but also its overall quality and accuracy. This chapter provides an overview of the fundamental parameters for data collection, as well as the calculation procedure. Detailed descriptions of each parameter can be found in [33].

MMS Data Acquisition

The test field was measured with a Riegl VMX-2HA mobile mapping instrument, attached to a car. The measurements were taken in December 2022. A panoramic camera was not used for the mapping as it was not planned to evaluate the photo data or colour the point clouds. The entire field was surveyed twice (forward and backward). The vehicle moved at an average speed of 20 km/h on the "forward" approach and 35 km/h on the "backward" approach. All significant parameters are listed in Table 3.

Tab.1 - Parameters of data collection

Environmental Factors	
Ambient Temperature	1 °C
Atmospheric Pressure	1020 hPa
Relative Humidity	90 %
Operational Parameters	
Average Vehicle Speed	20 km/h and 35 km/h
Laser Pulse Repeat Frequency	1000 kHz
Use of Panoramic Camera	Not utilized

MMS data processing

The Riegl RiPROCESS data software was used to create point clouds from the measured data and the trajectory from the GNSS/INS data was computed in the Applanix POSpac software. A total of eight point-clouds were computed, two clouds of the entire test field (forward and backward) with GCPs spacing 1km and two clouds for each Section in the same procedure. Figure 3 shows a flow chart of the process with important parameters.

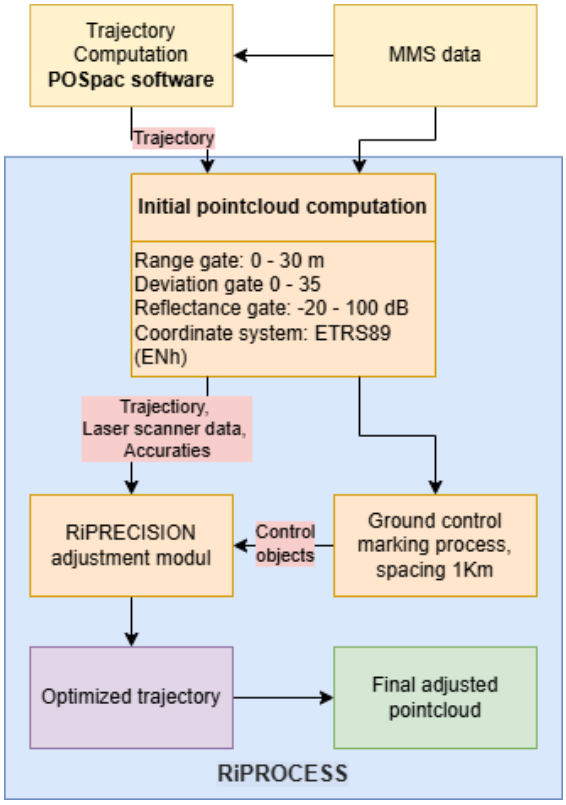

Fig.3 - Data processing flow chart

MMS evaluation

This chapter describes how the results are calculated and evaluated. It focusses on the influence of the alignment method in RiPROCESS software on the resulting cloud accuracy, the quality assumptions of GNSS point clouds, and in the last part to the point clouds and their accuracies.

Determination of accuracy

The deviations were determined by comparing the ground check points with the corresponding points extracted from the point clouds. Equation 1 provides the formula for calculating the Root Mean Square Error (RMSE), while Equation 2 defines the calculation of Standard Deviations.

$$RMSD = \sqrt{\frac{\sum_{i=1}^{n} \Delta x_i^2}{n}},$$

$$where\ \Delta x_i = X_i - \widehat{X}_i, X_i\ are\ the\ coordinates\ of\ the\ check\ point,$$

$$\widehat{X}_i\ are\ the\ coordinates\ of\ the\ point\ obtained\ from\ the\ point\ cloud. \quad (1)$$

$$StDev = \sqrt{\frac{\sum_{i=1}^{n} v_i^2}{n-1}},$$

$$where\ v_i^2 = \Delta\underline{X} - \Delta X_i,$$

$$\Delta X_i\ are\ the\ coordinators\ differences\ between\ the\ check\ points\ and\ the\ points\ obtained\ from\ the\ cloud,$$

$$\Delta\underline{X}\ is\ their\ average. \quad (2)$$

Influence of the Alignment Method

The initial trajectory is computed from GNSS, INS and DMI data. The absolute position is provided by GNSS, which, especially in places with obscured views of the sky, may show larger deviations from the actual terrain and in some places the trajectory may even be deformed. For these purposes, it is recommended to align the measurements with the ground control points and adjust the entire trajectory. The alignment process utilises GNSS, INS, and DMI data along with their respective accuracies. GCPs are marked on the initial point cloud to refine alignment.

Figure 4a shows the spatial deviations of the initial trajectory; the difference between sections and the impact of GNSS measurements on accuracy are significant. The state after the "non-rigid with translation" adjustment to the GCPs can be seen in Figure 4b. The marked locations of the local minima appear where the ground control points were located. There are four significant maximum deviations in this plot; these deviations are very similar to each other and occur at locations where the vehicle was forced to stop at the road junction. The last thing that can be noticed from comparing these two graphs is that the calculated deviations are reduced after the alignment, but the trends are kept. These graphs were computed in the RiPROCESS software.

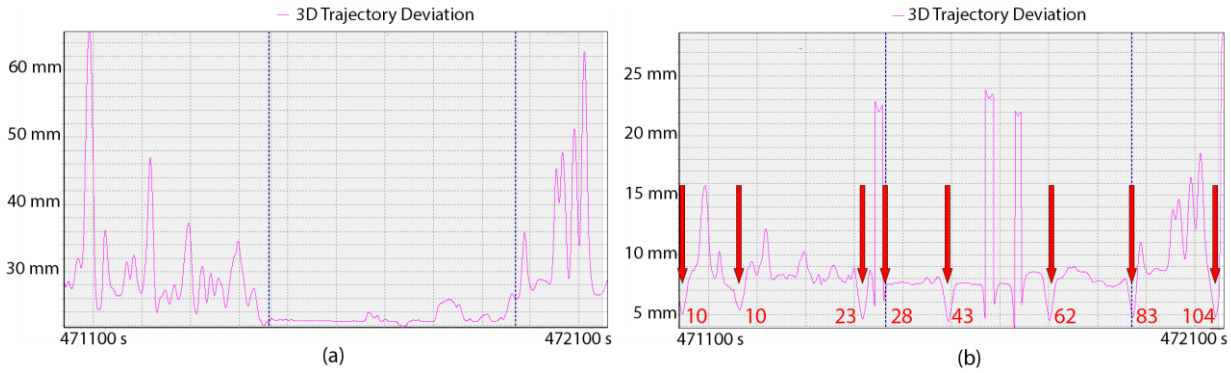

Fig.3 - RiProcess trajectory deviation

RiPRECISION software offers three types of adjustment:

Non-rigid with translation: The entire trajectory is first rotated and translated to minimise deviations at the ground control points, followed by local alignment around the ground control points, and therefore scale adjustment.

Non-rigid: Only local alignment around the ground control points and scale adjustment is performed.

Rigid with translation: The trajectory is rotated and translated to minimise deviations at the ground control points.

For comparison of the adjustment, the point clouds of Section 1 where the TS ground control points are used, and therefore the result will not include the GNSS error. Three clouds were computed, and each point cloud was first aligned at points 10 and 23 (1 km spacing between points), and the trajectories were adjusted according to the methods mentioned. Figure 5 shows the profile of point clouds with checkpoint TS 5.

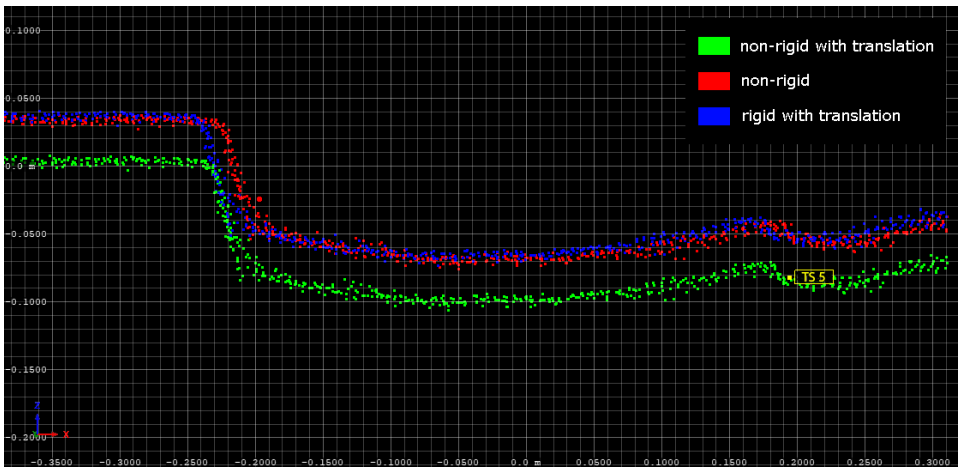

Fig.4 - Profile of various adjustment types

Accuracy of MMS in Various Environments

In this article, three types of environments are studied. The results are expected to show the difference in the point cloud accuracy with the same spacing of the GCPs. This section also focusses on the point cloud accuracy when the section was computed separately (without other sections) and when the section was computed together as one raid.

The last chapter is dedicated to the repeatability of measurements, i.e. the difference of point clouds of the same section that have been measured repeatedly and are tied on identical GCPs. The points taken from the "forward" and "backward" point clouds were compared. Also, in this case, differences were calculated from point clouds computed by sections and point clouds computed as part of the entire field.

RESULTS

Influence of the Alignment Method

Figure 6 illustrates the 3D deviations of each check points distributed along the trajectory. The deviations are calculated here as the difference between the TS point coordinate and a point manually taken from the point cloud. The plot values show similar trends in the deviations, especially between the "non-rigid" and "rigid with translation" methods. The "non-rigid with translation" method shows the smallest deviations during the trajectory, which can be seen in the summary of Table 4.

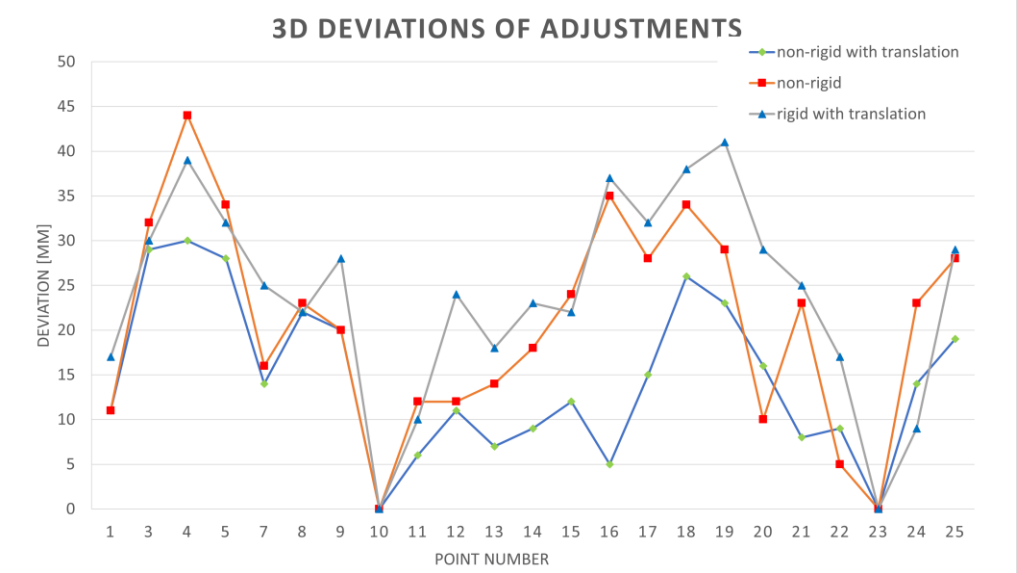

Fig. 5 - Points deviations of various adjustment types

Tab. 2 - Summary deviations of various adjustment types

Alignment method	StDev 3D [mm]	RMSD 3D [mm]
Non-rigid with translation	16	18
Non-rigid	20	25
Rigid with translation	20	27

Accuracy of MMS in Various Environments

Data collection was carried out in three areas. Section 1 was measured in a built-up urban area, Section 2 was carried out on a two-lane road section, without disturbing the view of the sky, and Section 3 data collection was carried out on a forested road. The sections are connected to each other.

Figure 7 shows the deviation plots for these sections. While the line graph represents the deviation of the MLS measured point from the "forward" approach from the point measured by GNSS method, the bar graphs show the 3D deviation of the points from the "forward" and "backward" passes. Compared to the GNSS points, the plot values also show the minimum deviation of the cloud calculated separately and the cloud computed as a group of all sections. The largest difference between these deviations can be seen in the graph of Section 2 at point 40, the difference reaches 26 mm.

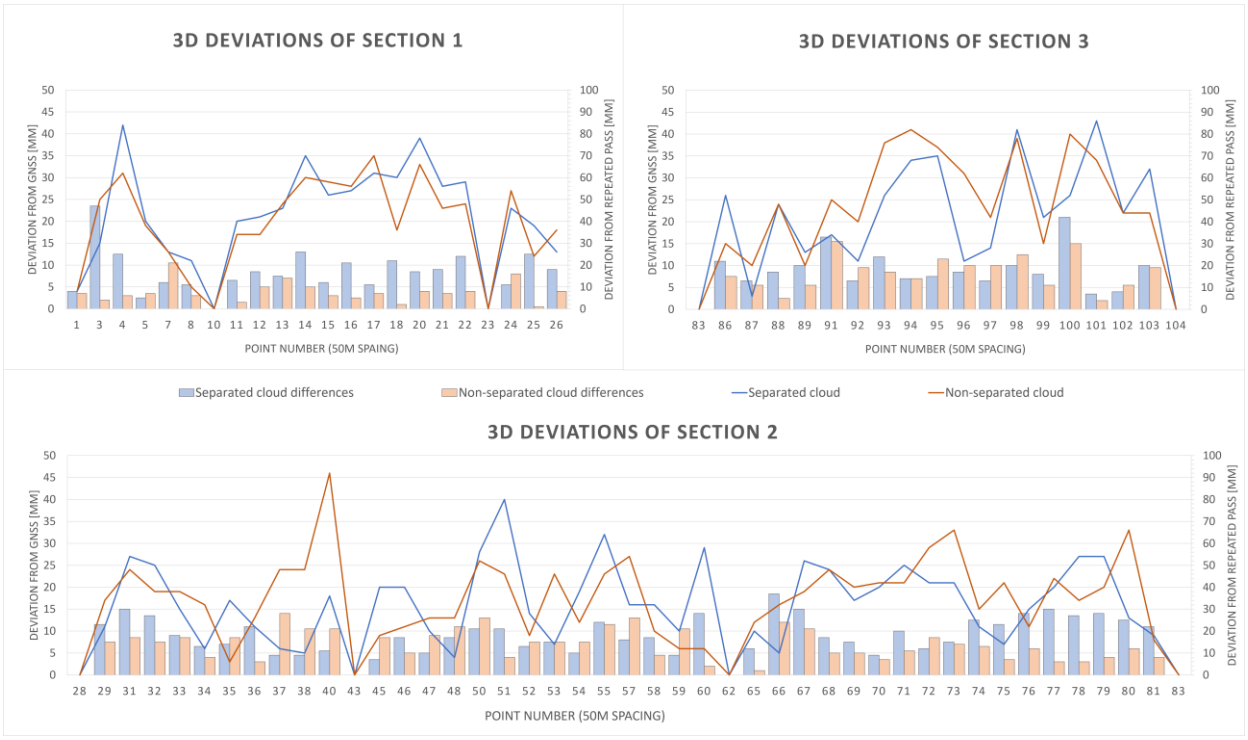

Fig.6 - Point deviations of measured sections

The Table 5 shows in detail the sampling standard deviations (StDev) and Root-mean-square-deviations (RMSD). The plane deviations of the first pass for all environments (compared with GNSS points) are almost identical, StDev 15mm. A more significant difference in this comparison is seen for spatial deviations, because of the height component. However, the difference in deviations between the areas is in the range of millimetres.

The difference in total deviations from the comparison of cloud points from two passes behaves similarly when the clouds are adjusted separately. For all environments, the deviations reach similar values. However, the table shows very small deviations in the height deviation when the clouds were calculated as part of the whole. The height deviations from these repeated passes are below 4 mm.

Tab. 3 - Summary deviations of measured sections

Section	Calc.	2D GNSS [mm]		3D GNSS [mm]		H GNSS [mm]	2D Rep. Pass [mm]		3D Rep. Pass [mm]		H Rep. Pass [mm]
		StDev	RMSD	StDev	RMSD	StDev	StDev	RMSD	StDev	RMSD	StDev
1	Sep.	16	17	21	24	13	14	16	17	19	10
	Tot.	15	17	20	22	13	9	9	9	9	2
2	Sep.	15	15	19	19	11	15	17	18	20	11
	Tot.	15	15	17	19	9	13	15	14	15	4
3	Sep.	15	16	23	27	17	16	19	17	20	6
	Tot.	16	18	21	25	12	15	19	15	19	1
Entire area	-	15	16	20	22	12	13	14	14	15	3

Explanatory notes:
Sep. - point clouds were calculated separately for each section, Tot. - point clouds were computed as part of the entire area.

CONCLUSION

This article was dedicated to comparing the accuracy of the MMS method with the Riegl VMX-2HA in various environments. These areas differed mainly in GNSS interference. The data were acquired on a 5.5 km long test field in Pilsen. The points used for the calculations are spaced at 50 m intervals along this route, and their coordinates were determined by the GNSS method.

In the first step, it was appropriate to determine the method of adjustment of the initial trajectory on the GCPs. An experiment was performed in which the measurements in the first section were aligned to two points (spaced 1000 m apart) and point clouds with different transformations were calculated. For these calculations, very precise points determined by the adjustment of the tied network (TS points) were used. The results show that the most accurate method and the method used further is the "non-rigid with translation" transformation, which achieved a 3D standard deviation of 16 mm.

The results of the sections comparison with GNSS points show several similar results. The first says that the accuracy of the point cloud, computed as part of the whole (with varying environments), increases the accuracy of the results. This was also applicable for Section 2, where linking to sections with worse conditions, there was no degradation in accuracy. The results show an improvement in the 3D standard deviation of 1-2 mm. The change of environment is only slightly reflected in the planar deviations, a more significant change is only seen in the elevation deviation, which affects the spatial accuracy. The best result in this experiment is the accuracy of Section 2 (road without GNSS interference) 3D StDev 17 mm, followed by the built-up area Section 1 3D StDev 20 mm and the forested road Section 3 3D StDev 21 mm.

The deviations from the repeat pass show spatial deviations of about 15 mm, and surprisingly the largest deviations in this comparison are in Section 2. Thus, it can be estimated that more weight was added to GNSS measurements (during MMS measurement) in this section, which were undisturbed here, making the calculation less dependent on the GCPs. An interesting value in this section is the standard deviation of the heights for point clouds computed as an entire area, here it is below the 5 mm. These values again suggest an improvement in accuracy when the sections are not separated.

The results of this work show the greater accuracy of the Riegl VMX-2HA, despite the density of GCPs, compared to its predecessor, the RIEGL VMX-450. The measurements show that this system can be reliably deployed under diverse conditions ranging from urban areas to forested roads. Its simplicity, fast data acquisition and precision make it a suitable primary method for mapping large areas without complex preparation or a high number of control points. The collected data can also be efficiently supplemented with outputs from handheld scanners, drone-based aerial surveys or conventional geodetic measurements. This approach helps to optimise the costs of spatial data collection while ensuring high quality of the final model.

ACKNOWLEDGEMENTS

This work was supported by the Grant Agency of the Czech Technical University in Prague, grants SGS25/046/OHK1/1T/11.

REFERENCES

[1] Chiang, K. W., Tsai, G. J., Zeng, J. C. 2021. Mobile mapping technologies. [online]. In: Urban Informatics. The Urban Book Series. p. 439–465. ISBN 978-981-15-8982-9. https://doi.org/10.1007/978-981-15-8983-6_25

[2] Lapucha, D. 1990. Precise GPS/INS “Positioning for Highway Inventory System”, Report No. 20038. Master’s thesis. [online]. Department of Geomatics Engineering, University of Calgary, Calgary (AB). http://hdl.handle.net/1880/18024
[3] El-Sheimy, N. 1996. The development of VISAT: a mobile survey system for GIS applications. Ph.D. thesis. [online]. University of Calgary, Calgary (AB), Canada. https://prism.ucalgary.ca
[4] Puente, I., González-Jorge, H., Martínez-Sánchez, J., Arias, P. 2013. Review of mobile mapping and surveying technologies. [online]. Measurement. vol. 46, no. 7, p. 2127–2145. ISSN 0263-2241. https://doi.org/10.1016/j.measurement.2013.03.006
[5] Kersting, A. P., Friess, P. 2016. Post-mission quality assurance procedure for survey-grade mobile mapping systems. [online]. The International Archives of the Photogrammetry, Remote Sensing and Spatial Information Sciences. 2016, vol. XLI-B1, p. 647–652. ISSN 2194-9034. Available at: https://doi.org/10.5194/isprs-archives-XLI-B1-647-2016
[6] Kaczmarek, A., Rohm, W.; Klingbeil, L., Tchórzewski, J. 2022. Experimental 2D extended Kalman filter sensor fusion for low-cost GNSS/IMU/odometers precise positioning system. [online]. Measurement. vol. 193, art. 110963. ISSN 0263-2241. https://doi.org/10.1016/j.measurement.2022.110963
[7] Blaser, S., Meyer, J., Nebiker, S., Fricker, L., Weber, D. 2020. Centimetre-accuracy in forests and urban canyons – combining a high-performance image-based mobile mapping backpack with new georeferencing methods. [online]. ISPRS Annals of the Photogrammetry, Remote Sensing and Spatial Information Sciences. vol. V-1-2020, p. 333–341. ISSN 2194-9050. https://doi.org/10.5194/isprs-annals-V-1-2020-333-2020
[8] Cavegn, S., Blaser, S., Nebiker, S., Haala, N. 2018. Robust and accurate image-based georeferencing exploiting relative orientation constraints. [online]. ISPRS Annals of the Photogrammetry, Remote Sensing and Spatial Information Sciences. vol. IV-2, p. 57–64. ISSN 2194-9050. https://doi.org/10.5194/isprs-annals-IV-2-57-2018
[9] Li, S., Li, G.; Wang, L., Qin, Y. 2020. SLAM integrated mobile mapping system in complex urban environments. [online]. ISPRS Journal of Photogrammetry and Remote Sensing. vol. 166, p. 316–332. ISSN 0924-2716. https://doi.org/10.1016/j.isprsjprs.2020.05.012
[10] Xu, X., Zhang, L., Yang, J., Cao, C., Wang, W. et al. 2022. A review of multi-sensor fusion SLAM systems based on 3D LiDAR. [online]. Remote Sensing. vol. 14, no. 12, art. 2835. ISSN 2072-4292. https://doi.org/10.3390/rs14122835
[11] Gharineiat, Z., Tarsha Kurdi, F., Henny, K., Gray, H., Jamieson, A. et al. 2024. Assessment of NavVis VLX and BLK2GO SLAM scanner accuracy for outdoor and indoor surveying tasks. [online]. Remote Sensing. vol. 16, no. 17, art. 3256. ISSN 2072-4292. https://doi.org/10.3390/rs16173256
[12] Vynikal, J., Zahradník, D. 2023. Floor plan creation using a low-cost 360° camera. [online]. The Photogrammetric Record., vol. 38, no. 184, p. 520–536. ISSN 0031-868X. https://doi.org/10.1111/phor.12463
[13] Oniga, V. E., Breaban, A. I., Alexe, E. I., Văsii, C. 2021. Indoor mapping of a complex cultural heritage scene using TLS and HMLS laser scanning. [online]. The International Archives of the Photogrammetry, Remote Sensing and Spatial Information Sciences., vol. XLIII-B2-2021, p. 605–612. ISSN 2194-9034. https://doi.org/10.5194/isprs-archives-XLIII-B2-2021-605-2021
[14] Chudá, J., Výbošťok, J., Tomaštík, J., Chudý, F., Tunák, D. et al. 2024. Prompt mapping tree positions with handheld mobile scanners based on SLAM technology. [online]. Land., vol. 13, no. 1, art. 93. ISSN 2073-445X. https://doi.org/10.3390/land13010093
[15] Pavelka, K., Matoušková, E., Pavelka, K. 2023. Remarks on geomatics measurement methods focused on forestry inventory. [online]. Sensors., vol. 23, no. 17, art. 7376. ISSN 1424-8220. https://doi.org/10.3390/s23177376
[16] Pavelka, K., Pavelka, K., Matoušková, E., Smolík, T. 2021. Earthen Jewish Architecture of Southern Morocco: Documentation of Unfired Brick Synagogues and Mellahs in the Drâa-Tafilalet Region, Applied Sciences., 11(4), 1-25. ISSN 2076-3417. https://doi.org/10.3390/app11041712
[17] Trybała, P., Kasza, D., Wajs, J., Remondino, F. 2023. Comparison of low-cost handheld LiDAR-based SLAM systems for mapping underground tunnels. [online]. The International Archives of the Photogrammetry, Remote Sensing and Spatial Information Sciences., vol. XLVIII-1/W1-2023, p. 517–524. ISSN 2194-9034. https://doi.org/10.5194/isprs-archives-XLVIII-1-W1-2023-517-2023

[18] Di Stefano, F., Chiappini, S., Gorreja, A., Balestra, M., Pierdicca, R. 2021. Mobile 3D scan LiDAR: a literature review. [online]. Geomatics, Natural Hazards and Risk., vol. 12, no. 1, p. 2387–2429. ISSN 1947-5705. https://doi.org/10.1080/19475705.2021.1964617
[19] Yang, B., Dong, Z., Liu, Y., Liang, F., Wang, Y. 2017. Computing multiple aggregation levels and contextual features for road facilities recognition using mobile laser scanning data. [online]. ISPRS Journal of Photogrammetry and Remote Sensing., vol. 126, p. 180–194. ISSN 0924-2716. https://doi.org/10.1016/j.isprsjprs.2017.02.014
[20] Wang, H., Luo, H., Wen, C., Cheng, J., Li, P. et al. 2015. Road boundaries detection based on local normal saliency from mobile laser scanning data. [online]. IEEE Geoscience and Remote Sensing Letters., vol. 12, no. 10, p. 2085–2089. ISSN 1545-598X. https://doi.org/10.1109/LGRS.2015.2449074
[21] Balado, J., Díaz-Vilariño, L., Arias, P., González-Jorge, H. 2018. Automatic classification of urban ground elements from mobile laser scanning data. [online]. Automation in Construction, vol. 86, p. 226–239. ISSN 0926-5805. https://doi.org/10.1016/j.autcon.2017.09.004
[22] Guney, E., Bayilmis, C., Çakan, B. 2022. An implementation of real-time traffic signs and road objects detection based on mobile GPU platforms. [online]. IEEE Access, vol. 10, p. 86191–86203. ISSN 2169-3536. https://doi.org/10.1109/ACCESS.2022.3198954
[23] Ma, Y., Zheng, Y., Easa, S., Wong, Y. D., El-Basyouny, K. 2022. Virtual analysis of urban road visibility using mobile laser scanning data and deep learning. [online]. Automation in Construction, Vol.133, Elsevier, ISSN: 0926-5805, https://doi.org/10.1016/j.autcon.2021.104014
[24] Ma, L., Li, Y., Li, J., Junior, J. M., Goncalves, W. N. et al. 2022. BoundaryNet: extraction and completion of road boundaries with deep learning using mobile laser scanning point clouds and satellite imagery. [online]. IEEE Transactions on Intelligent Transportation Systems., vol. 23, no. 6, p. 5638–5654. ISSN 1524-9050. https://doi.org/10.1109/TITS.2021.3055366
[25] Yao, L., Qin, C., Chen, Q., Wu, H. 2021. Automatic Road marking extraction and vectorization from vehicle-borne laser scanning data. [online]. Remote Sensing., vol. 13, no. 13, art. 2612. ISSN 2072-4292. https://doi.org/10.3390/rs13132612
[26] Li, Q., Yuan, P., Lin, Y., Tong, Y., Liu, X. 2021. Pointwise classification of mobile laser scanning point clouds of urban scenes using raw data. [online]. Journal of Applied Remote Sensing, vol. 15, no. 2, art. 024523. ISSN 1931-3195. https://doi.org/10.1117/1.JRS.15.024523
[27] Reiterer, A., Wäschle, K., Störk, D., Leydecker, A., Gitzen, N. 2020. Fully automated segmentation of 2D and 3D mobile mapping data for reliable modeling of surface structures using deep learning. [online]. Remote Sensing., vol. 12, no. 16, art. 2530. ISSN 2072-4292. https://doi.org/10.3390/rs12162530
[28] Vierhub-Lorenz, V., Kellner, M., Zipfel, O., Reiterer, A. 2022. A study on the effect of multispectral LiDAR data on automated semantic segmentation of 3D point clouds. [online]. Remote Sensing, vol. 14, no. 24, art. 6349. ISSN 2072-4292. https://doi.org/10.3390/rs14246349
[29] Kalvoda, P., Nosek, J., Kuruc, M., Volarik, T., Kalvodova, P. 2020. Accuracy evaluation and comparison of mobile laser scanning and mobile photogrammetry data. [online]. IOP Conference Series: Earth and Environmental Science., vol. 609, no. 1, art. 012091. ISSN 1755-1307. https://doi.org/10.1088/1755-1315/609/1/012091
[30] Puente, I., González-Jorge, H., Riveiro, B., Arias, P. 2013. Accuracy verification of the Lynx mobile mapper system. [online]. Optics & Laser Technology., vol. 45, p. 578–586. ISSN 0030-3992. https://doi.org/10.1016/j.optlastec.2012.05.029
[31] Grešla, O., Jašek, P. 2023. Measuring Road structures using a mobile mapping system. [online]. The International Archives of the Photogrammetry, Remote Sensing and Spatial Information Sciences., vol. XLVIII-5/W2-2023, p. 43–48. ISSN 2194-9034. https://doi.org/10.5194/isprs-archives-XLVIII-5-W2-2023-43-2023
[32] Treccani, D., Adami, A., Brunelli, V., Fregonese, L. 2024. Mobile mapping system for historic built heritage and GIS integration: a challenging case study. [online]. Applied Geomatics., vol. 16, no. 1, p. 293–312. ISSN 1866-9298. https://doi.org/10.1007/s12518-024-00555-w
[33] Běloch, L., Pavelka, K. 2024. Optimizing mobile laser scanning accuracy for urban applications: a comparison by strategy of different measured ground points. [online]. Applied Sciences, vol. 14, no. 8, art. 3387. ISSN 2076-3417. https://doi.org/10.3390/app14083387

[34] Kalvoda, P., Nosek, J., Kalvodova, P. 2021. Influence of control points configuration on the mobile laser scanning accuracy. [online]. IOP Conference Series: Earth and Environmental Science., vol. 906, no. 1, art. 012091. ISSN 1755-1307. https://doi.org/10.1088/1755-1315/906/1/012091

[35] Grešla, O. 2024. Experimental determination of the influence of choosing tie points for mobile mapping in poor conditions. [online]. Geodesy in construction and industry. Prague: Czech Association of Surveyors and Cartographers (Geodézie ve stavebnictví a průmyslu. Praha: Český svaz geodetů a kartografů), p. 70–80. ISBN 978-80-02-03049-2. http://csgk.fce.vutbr.cz/Oakce/A139/prezentace/11_GSP24_Gresla.pdf [accessed 2025-02-15].

[36] Mattheuwsen, L., Bassier, M., Vergauwen, M. 2019. Theoretical accuracy prediction and validation of low-end and high-end mobile mapping system in urban, residential and rural areas. [online]. The International Archives of the Photogrammetry, Remote Sensing and Spatial Information Sciences., vol. XLII-2/W18, p. 121–128. ISSN 2194-9034. https://doi.org/10.5194/isprs-archives-XLII-2-W18-121-2019